

See discussions, stats, and author profiles for this publication at: <https://www.researchgate.net/publication/307880289>

A practical comparison of different parameterizations for anisotropic elastic full-waveform inversion

Conference Paper · September 2016

DOI: 10.1190/segam2016-13944676.1

CITATIONS

0

READS

27

3 authors, including:



Espen Birger Raknes

Norwegian University of Science and Technology

17 PUBLICATIONS 37 CITATIONS

[SEE PROFILE](#)



Børge Arntsen

Norwegian University of Science and Technology

129 PUBLICATIONS 531 CITATIONS

[SEE PROFILE](#)

Some of the authors of this publication are also working on these related projects:



Project

Full Wave Seismic-Acoustic Propagation modelling: Horizontl/Vertical Arrays [View project](#)

A practical comparison of different parameterizations for anisotropic elastic full waveform inversion

Tore S. Bergslid*, Espen Birger Raknes and Børge Arntsen, Norwegian University of Science and Technology

SUMMARY

In elastic anisotropic FWI, choosing the optimal parameterization for a problem is important. We have compared the results of using three different parameterizations when performing elastic anisotropic FWI. The parameterizations are: 1) V_{P0} , V_{S0} , ε , δ , 2) V_{P0} , V_{S0} , V_{hor} , V_{nmo} , 3) V_{P0} , V_{S0} , η , δ . Experiments have been run on complex and simple models. Results indicate that with our survey geometry, crosstalk is still an issue for all three parameterizations. An additional problem with parameterizations one and three is the difference in amplitude between the velocities and anisotropy parameters, that leads to issues updating anisotropy parameters for multiparameter inversion.

INTRODUCTION

Full-waveform inversion (FWI) is a technique for estimating subsurface properties by using the entire recorded waveform and applying inverse theory (Tarantola (1984), Mora (1987)). If the elastic effects have a weak signature in the data, acoustic FWI can work well (Brossier et al. (2009)). At the present time, anisotropic FWI is still mostly performed using the acoustic approximation (Warner et al. (2013), Plessix et al. (2014)).

Anisotropic media are described by stiffness coefficients. In the case of elastic 2D vertical transverse isotropy (VTI) we have four such coefficients, in addition to density. These can be combined in various ways to create different parameterizations. Most common is using density (ρ), vertical P-wave velocity (V_{P0}), vertical S-wave velocity (V_{S0}), and Thomsen parameters ε and δ (Thomsen (1986)). However, these are not necessarily the best parameters to use in FWI. Multiparameter anisotropic elastic FWI is a highly non-linear problem. The optimal set of parameters can reduce crosstalk between parameters and improve results.

Gholami et al. (2013) showed that the choice of parameterization is important for acoustic anisotropic FWI. Alkhalifah and Plessix (2014) describes two parameterizations that are good for acoustic FWI in VTI media: 1) P-wave NMO velocity ($V_{\text{nmo}} = V_{P0}\sqrt{1+2\delta}$), anisotropy parameters δ and $\eta = (\varepsilon - \delta)/(1+2\delta)$, 2) horizontal P-wave velocity ($V_{\text{hor}} = V_{P0}\sqrt{1+2\varepsilon}$), η and ε .

Recovering the Thomsen parameters ε and δ in homogeneous media by inverting for the vertical S-wave velocity (V_{S0}), V_{P0} , V_{nmo} and V_{hor} and then calculating ε and δ from the results has been shown to be possible (Kamath and Tsvankin (2014), Kamath and Tsvankin (2016)). In our previous work (Bergslid et al. (2015)) we showed that it is possible to invert directly for ε and δ in more complex models with long offset data.

In this study, the goal is to directly compare the results of anisotropic elastic full waveform inversion when using differ-

ent parameterizations: 1) V_{P0} , V_{S0} , ε , δ , 2) V_{P0} , V_{S0} , V_{hor} , V_{nmo} , 3) V_{P0} , V_{S0} , η , δ . The third parameterization is an extension of Alkhalifah and Plessix (2014) to the elastic case by also including V_{S0} . These parameterizations were chosen based on the fact that there exists previous work showing that each of them can work in VTI FWI. V_{P0} -inversions are run for a complex model with a decent V_{P0} starting model, and multiparameter inversion is performed on a simple homogeneous model with a perturbation in V_{P0} or ε .

THEORY

Using the Einstein summation convention, the elastic wave equation can be written in the following form:

$$\rho \ddot{u}_i - \partial_j c_{ijkl} \partial_l u_k = f_i, \quad (1a)$$

$$c_{ijkl} \partial_l u_k n_j = T_i. \quad (1b)$$

where $u_i = u_i(\mathbf{x}_s, \mathbf{x}, t)$ is the i th component of displacement resulting from a shot (i.e., body force f_i and/or traction T_i) located at \mathbf{x}_s , c_{ijkl} is the stiffness tensor, n_j is a normal vector and ρ is the density.

In FWI the goal is to iteratively update our starting model towards the true model. We therefore define a measure, $\mathcal{F}(\mathbf{m})$, between the modeled data \mathbf{u} and the measured data \mathbf{d} . This measure is often called the misfit functional, and is here defined as follows (Raknes and Arntsen (2014)):

$$\mathcal{F}(\mathbf{m}) = \frac{1}{2} \sum_{j=0}^{n_s} \sum_{i=0}^{n_r} \|\hat{\mathbf{u}}_{i,j}(\mathbf{m}) - \hat{\mathbf{d}}_{i,j}\|_2^2, \quad (2)$$

where $\hat{\mathbf{u}}_{i,j}(\mathbf{m}) = \mathbf{u}_{i,j}(\mathbf{m}) / \|\mathbf{u}_{i,j}(\mathbf{m})\|_2$ is the normalized modeled data, $\hat{\mathbf{d}}_{i,j} = \mathbf{d}_{i,j} / \|\mathbf{d}_{i,j}\|_2$ is the normalized measured data, n_r is the number of receivers in the data set and n_s is the number of shots. $\|\cdot\|_2$ refers to the L^2 -norm.

The crucial step in FWI is computing the gradient. Finding expressions for the gradients in a VTI medium is done by following the approach of Mora (1987), but assuming VTI medium. Writing out the stiffness tensor c_{ijkl} for VTI, the expressions for the model update gradients with respect to the stiffness coefficients in 2D can be found:

$$\begin{aligned} \hat{\delta}\rho &= - \sum_{n_s} \int dt \hat{u}_j \Psi_j, \\ \hat{\delta}c_{11} &= - \sum_{n_s} \int dt u_{1,1} \Psi_{1,1}, \\ \hat{\delta}c_{33} &= - \sum_{n_s} \int dt u_{3,3} \Psi_{3,3}, \\ \hat{\delta}c_{13} &= - \sum_{n_s} \int dt (\Psi_{3,3} u_{1,1} + \Psi_{1,1} u_{3,3}), \\ \hat{\delta}c_{44} &= - \sum_{n_s} \int dt (\Psi_{3,1} + \Psi_{1,3})(u_{3,1} + u_{1,3}). \end{aligned} \quad (3)$$

Parameterization comparisons VTI EFWI

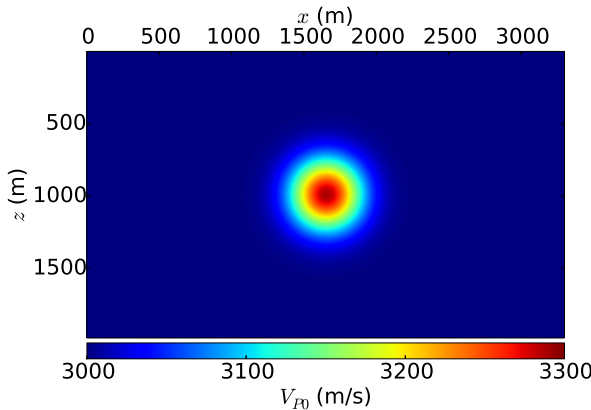


Figure 1: True V_{P0} perturbation.

Here, $u_{i,j}$ is the derivative in the j -direction of the forward modelled field in the i -direction. $\Psi_{i,j}$ is the equivalent for the backward modelled field. In order to find the gradients in terms of our various parameterizations, a change of variables is required. Parameterization one gives the following gradients:

$$\begin{aligned} \hat{\delta}V_{P0} &= 2\rho V_{P0}(1+2\epsilon)\hat{\delta}c_{11} \\ &+ 2\rho V_{P0} \frac{V_{P0}^2 - V_{S0}^2 + \delta(2V_{P0}^2 - V_{S0}^2)}{\sqrt{(V_{P0}^2 - V_{S0}^2)^2 + 2\delta V_{P0}^2(V_{P0}^2 - V_{S0}^2)}} \hat{\delta}c_{13} \\ &+ 2\rho V_{P0}\hat{\delta}c_{33}, \\ \hat{\delta}V_{S0} &= 2\rho V_{S0} \left[\frac{V_{S0}^2 - V_{P0}^2 - \delta V_{P0}^2}{\sqrt{(V_{P0}^2 - V_{S0}^2)^2 + 2\delta V_{P0}^2(V_{P0}^2 - V_{S0}^2)}} \right. \\ &\quad \left. - 1 \right] \hat{\delta}c_{13} + 2\rho V_{S0}\hat{\delta}c_{44}, \\ \hat{\delta}\epsilon &= 2\rho V_{P0}^2\hat{\delta}c_{11}, \\ \hat{\delta}\delta &= \rho \frac{V_{P0}^2(V_{P0}^2 - V_{S0}^2)}{\sqrt{(V_{P0}^2 - V_{S0}^2)^2 + 2\delta V_{P0}^2(V_{P0}^2 - V_{S0}^2)}} \hat{\delta}c_{13}. \end{aligned} \quad (4)$$

For parameterization two, the gradients are

$$\begin{aligned} \hat{\delta}V_{P0} &= \rho V_{P0} \frac{V_{nmo}^2 - V_{S0}^2}{\sqrt{(V_{nmo}^2 - V_{S0}^2)(V_{P0}^2 - V_{S0}^2)}} \hat{\delta}c_{13} \\ &+ 2\rho V_{P0}\hat{\delta}c_{33}, \\ \hat{\delta}V_{S0} &= 2\rho V_{S0} \left[\frac{V_{S0}^2 - 0.5(V_{P0}^2 - V_{nmo}^2)}{\sqrt{(V_{nmo}^2 - V_{S0}^2)(V_{P0}^2 - V_{S0}^2)}} - 1 \right] \hat{\delta}c_{13} \\ &+ 2\rho V_{S0}\hat{\delta}c_{44}, \\ \hat{\delta}V_{hor} &= 2\rho V_{hor}\hat{\delta}c_{11}, \\ \hat{\delta}V_{nmo} &= \rho V_{nmo} \frac{V_{P0}^2 - V_{S0}^2}{\sqrt{(V_{nmo}^2 - V_{S0}^2)(V_{P0}^2 - V_{S0}^2)}} \hat{\delta}c_{13}. \end{aligned} \quad (5)$$

Parameterization three has gradients given by

$$\begin{aligned} \hat{\delta}V_{nmo} &= 2\rho V_{nmo}(1+2\eta)\hat{\delta}c_{11} \\ &+ 2\rho V_{nmo} \sqrt{\frac{V_{nmo}^2 - V_{S0}^2(1+2\delta)}{V_{nmo}^2 - V_{S0}^2(1+2\delta) + 2\delta V_{nmo}^2}} \hat{\delta}c_{13} \end{aligned}$$

$$\begin{aligned} &+ \frac{2\rho V_{nmo}}{1+2\delta} \hat{\delta}c_{33}, \\ \hat{\delta}V_{S0} &= 2\rho V_{S0} \\ &\left[\frac{V_{S0}^2(1+2\delta) - V_{nmo}^2(1+\delta)}{\sqrt{(V_{nmo}^2 - V_{S0}^2(1+2\delta))^2 + 2\delta V_{nmo}^2(V_{nmo}^2 - V_{S0}^2(1+2\delta))}} - 1 \right] \hat{\delta}c_{13}, \\ &+ 2\rho V_{S0}\hat{\delta}c_{44}, \\ \hat{\delta}\eta &= 2\rho V_{nmo}^2\hat{\delta}c_{11}, \\ \hat{\delta}\delta &= \frac{\rho V_{nmo}^2}{1+2\delta} \\ &\left[\frac{V_{S0}^2 - V_{nmo}^2}{\sqrt{(V_{nmo}^2 - V_{S0}^2(1+2\delta))^2 + 2\delta V_{nmo}^2(V_{nmo}^2 - V_{S0}^2(1+2\delta))}} \right] \hat{\delta}c_{13} \\ &- \frac{2\rho V_{nmo}^2}{(1+2\delta)^2} \hat{\delta}c_{33}. \end{aligned} \quad (6)$$

Minimizing the misfit functional in eq. (2) is done via the limited-memory Broyden-Fletcher-Goldfarb-Shanno (L-BFGS) algorithm (Nocedal and Wright (2006)), which is a quasi-Newton method that uses gradients from previous iterations to estimate the inverse Hessian matrix.

RESULTS

The complex geology example was a synthetic model of the Gullfaks field, including ϵ and δ , with the same starting model as in our previous work (Bergslid et al. (2015)). Receivers and shots were placed in the water layer at 10 m depth. The grid spacing was 10 m in both directions, with receivers every 10 m in the x-direction and shots every 100 m. A Ricker wavelet with a center frequency of 5 Hz was used as the source. Only pressure data were used.

There is one key difference between the gradients in the three parameterizations: V_{P0} in parameterization two is not dependent on $\hat{\delta}c_{11}$, whereas V_{P0} in parameterization one and V_{nmo} in parameterization three are. For every other parameter except δ in parameterization three, which has an additional dependence on $\hat{\delta}c_{33}$, there is a corresponding parameter in each parameterization that depends on the same wavefield components. Since $\hat{\delta}c_{11}$ is a term that contains information about the horizontal component of the wavefields, examining its effect on long offset FWI would be interesting. Therefore, with this model, we have focused on inverting for V_{P0} in the case of parameterizations one and two, and for V_{nmo} with parameterization three.

Results from the V_{P0} inversions in the complex model are shown in Fig. 2. It is clear that parameterizations one and three worked well for this example. However, parameterization two produced artifacts near the surface as well as wrong updates in the low velocity layer at 1000 to 1500 m. The linesearch criterion had to be relaxed in order for parameterization two to start iterating at all, which allowed the inversion to get stuck in a local minimum. In a long offset case such as this, it appears this horizontal component is critical in order to guide the inversion towards the correct solution if the starting model is not very close.

Parameterization comparisons VTI EFWI

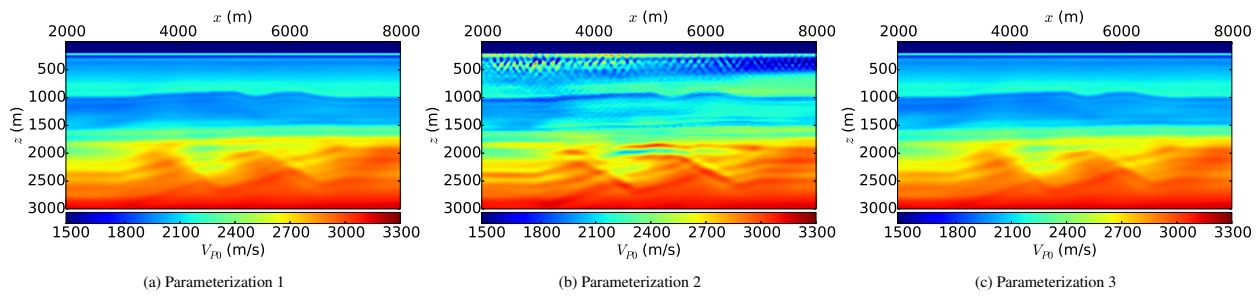


Figure 2: V_{P0} inversion results for the Gullfaks model in each of the three parameterizations.

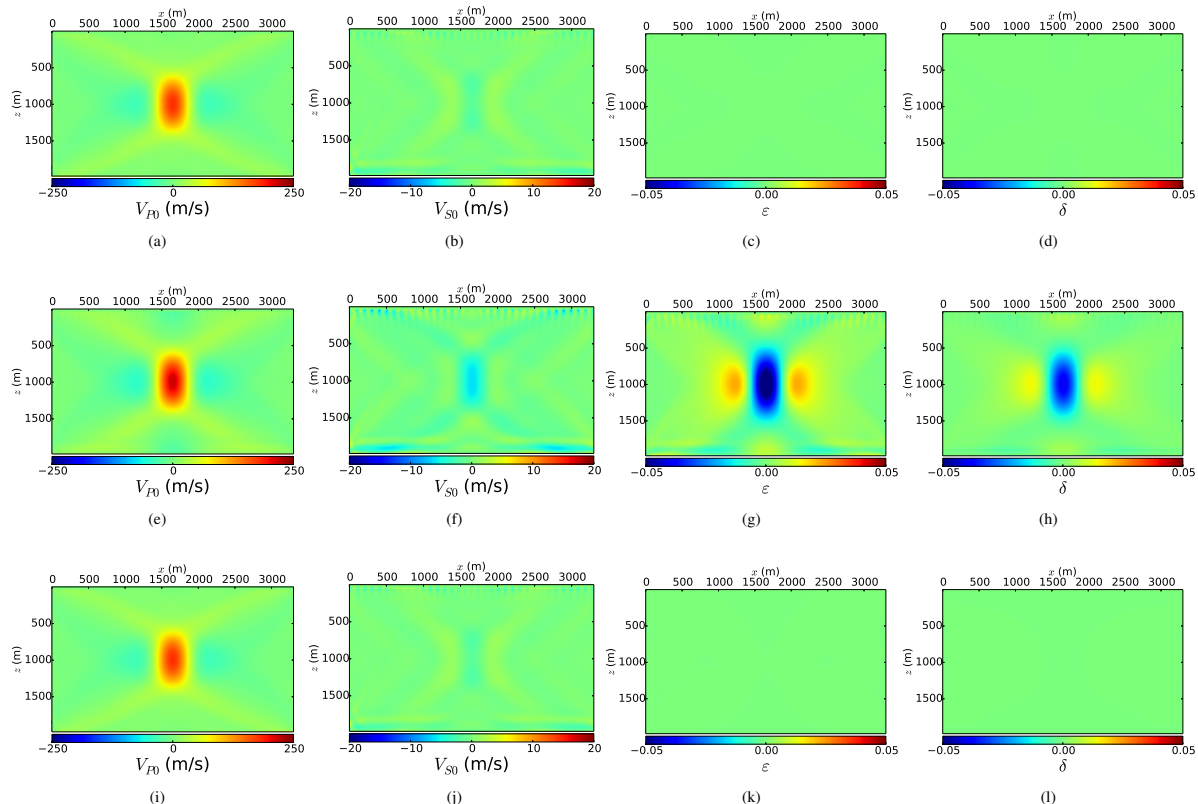


Figure 3: Difference between initial and final models with a perturbation in V_{P0} . (a) – (d): parameterization 1, (e) – (h): parameterization 2, (i) – (l): parameterization 3

A simpler model was used to examine the crosstalk between different parameters. This was done using multicomponent transmission data and inverting for all four parameters at the same time. A circular decaying anomaly in V_{P0} with a maximum magnitude of 288 m/s (Fig. 1) was placed in the middle of the model, shots were spaced by approximately 100 meters close to the top, and receivers were placed in every grid point along the bottom of the model. The source was a Ricker wavelet with a center frequency of 10 Hz. Homogeneous parameters were chosen similar to Kamath and Tsvankin (2014): $V_{P0} = 3000$ m/s, $V_{S0} = 1500$ m/s, $\epsilon = 0.1$ and $\delta = -0.05$. The numerical model is a 300×500 grid, with a grid spacing of 6.6

m in both directions. True homogeneous models were used as starting models. For the experiment with the anomaly in ϵ , the anomaly had the same form as for V_{P0} , with a maximum value of 0.143.

Fig. 3 shows the results for the inversion with an anomaly in V_{P0} . Both parameterizations one and three were able to recover approximately 63% of the maximum value of the true anomaly, Fig. 3a and 3i, with insignificant updates to the other parameters. Parameterization two stands out here, as it managed to recover 75% of the maximum. However, the updates in V_{hor} and V_{nmo} are not as well behaved, leading to large erroneous updates in ϵ (-0.058) and δ (-0.04). This result agrees

Parameterization comparisons VTI EFWI

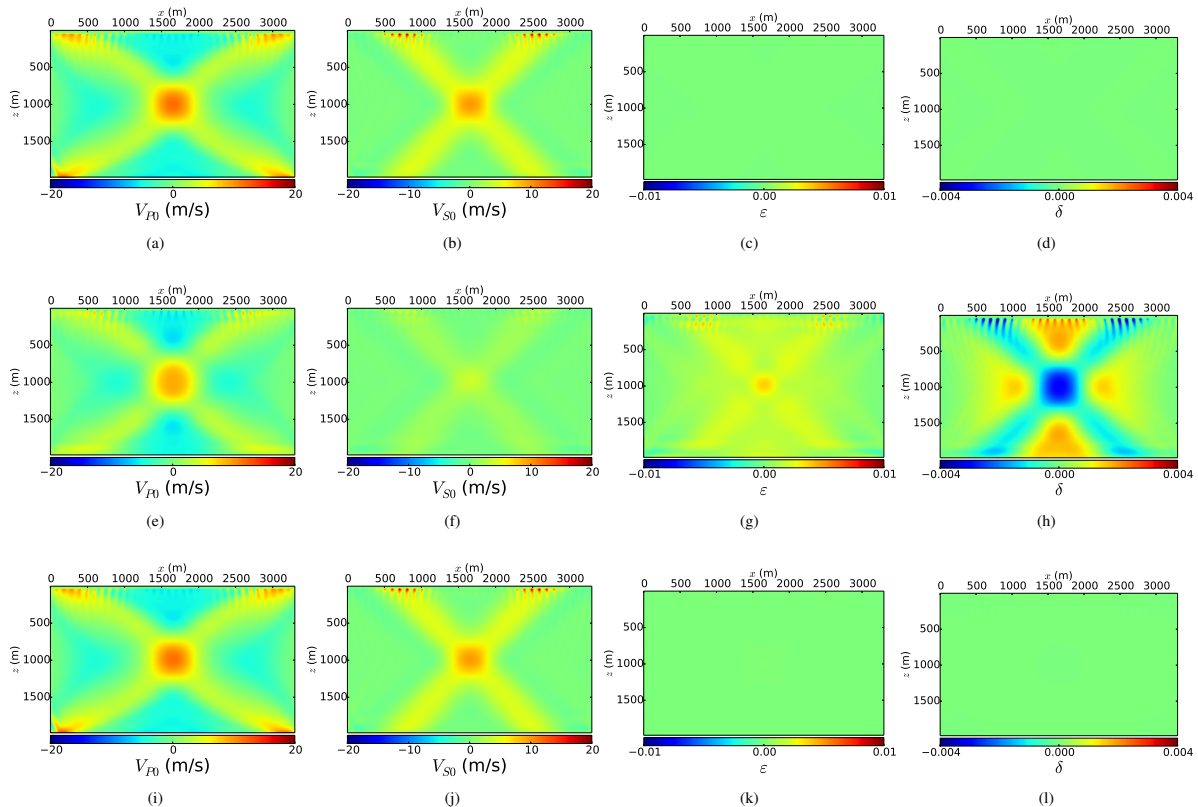


Figure 4: Difference between initial and final models with a perturbation in ε . (a) – (d): parameterization 1, (e) – (h): parameterization 2,(i) – (l): parameterization 3

with Kamath and Tsvankin (2014).

Since ε governs the horizontal P-wave velocity, a vertical transmission experiment is clearly a suboptimal survey geometry in order to recover the true ε . As such, a good recovery of the true anomaly is not expected.

Results of the inversion with the anomaly in ε can be seen in Fig. 4. Parameterizations one and three give almost identical results, and neither is able to capture the anomaly in any meaningful way, instead trying to compensate by updating V_{P0} and V_{S0} . Parameterization two does slightly better by both performing smaller updates in V_{P0} and V_{S0} as well as actually beginning to recover the anomaly, albeit only at approximately 10% of the true value. An incorrect update of δ occurs here as well.

In both experiments with the simple model, parameterizations one and three did not perform any significant updates to ε and δ . Due to keeping the color scale consistent between parameterizations, the small changes that were done are not visible in the figures. However, the updates still recover the structure of the anomaly, but the amplitude is tiny. This could be a result of the amplitude difference between the velocities and the anisotropy parameters causing issues when inverting for all parameters at the same time. As parameterization two only uses velocities, it does not encounter the same problem.

CONCLUSIONS

In this study we have performed multiparameter FWI of multi-component transmission data in simple models as well as V_{P0} inversion in a complex model, using three different model parameterizations in each example. The V_{P0} inversions show that using a parameterization that includes as much information as possible about the horizontal component of the wavefields in the gradient when inverting for V_{P0} with long offset data can mean the difference between recovering a good model or not. Experiments using the simple models demonstrate significant crosstalk between parameters in parameterization two. Parameterizations one and three have problems updating anisotropy parameters in multiparameter inversion, likely as a consequence of the amplitude difference between velocities and anisotropy parameters.

ACKNOWLEDGMENTS

The authors thank the ROSE consortium and their sponsors for support.

EDITED REFERENCES

Note: This reference list is a copyedited version of the reference list submitted by the author. Reference lists for the 2016 SEG Technical Program Expanded Abstracts have been copyedited so that references provided with the online metadata for each paper will achieve a high degree of linking to cited sources that appear on the Web.

REFERENCES

- Alkhalifah, T., and R.-E. Plessix, 2014, A recipe for practical full-waveform inversion in anisotropic media: An analytical parameter resolution study: *Geophysics*, **79**, no. 3, R91–R101, <http://dx.doi.org/10.1190/geo2013-0366.1>.
- Bergslid, T. S., E. B. Raknes, and B. Arntsen, 2015, The influence of anisotropy on elastic full-waveform inversion: 85th Annual International Meeting, SEG, Expanded Abstracts, 1425–1429, <http://dx.doi.org/10.1190/segam2015-5897724.1>.
- Brossier, R., S. Operto, J. Virieux, 2009, Two-dimensional seismic imaging of the valhall model from synthetic obc data by frequency-domain elastic full-waveform inversion: 79th Annual International Meeting, SEG, Expanded Abstracts, 28, 2293–2297, <http://dx.doi.org/10.1190/1.3255318>.
- Gholami, Y., R. Brossier, S. Operto, A. Ribodetti, and J. Virieux, 2013, Which parameterization is suitable for acoustic vertical transverse isotropic full waveform inversion? part 1: Sensitivity and trade-off analysis: *Geophysics*, **78**, no. 2, R81–R105, <http://dx.doi.org/10.1190/geo2012-0204.1>.
- Kamath, N., and I. Tsвvakin, 2014, Elastic full-waveform inversion of transmission data in 2d VTI media: 84th Annual International Meeting, SEG, Expanded Abstracts, <http://dx.doi.org/10.1190/segam2014-0869.1>.
- Kamath, N., and I. Tsвvakin, 2016, Elastic full-waveform inversion for VTI media: Methodology and sensitivity analysis: *Geophysics*, **81**, no. 2, C53–C68, <http://dx.doi.org/10.1190/geo2014-0586.1>.
- Mora, P., 1987, Nonlinear two-dimensional elastic inversion of multioffset seismic data: *Geophysics*, **52**, 1211–1228, <http://dx.doi.org/10.1190/1.1442384>.
- Nocedal, J., and S. J. Wright, 2006, Numerical optimization, 2nd ed.: Springer, 497–528.
- Plessix, R.-E., A. Stopin, P. Milcik, and K. Matson, 2014, Acoustic and anisotropic multi-parameter seismic full waveform inversion case studies: 84th Annual International Meeting, SEG, Expanded Abstracts, <http://dx.doi.org/10.1190/segam2014-0646.1>.
- Raknes, E. B., and B. Arntsen, 2014, Time-lapse full-waveform inversion of limited-offset seismic data using a local migration regularization: *Geophysics*, **79**, no. 3, WA117–WA128, <http://dx.doi.org/10.1190/geo2013-0369.1>.
- Tarantola, A., 1984, Inversion of seismic reflection data in the acoustic approximation: *Geophysics*, **49**, 1259–1266, <http://dx.doi.org/10.1190/1.1441754>.
- Thomsen, L., 1986, Weak elastic anisotropy: *Geophysics*, **51**, 1954–1966, <http://dx.doi.org/10.1190/1.1442051>.
- Warner, M. A., T. Ratcliffe, J. Nangoo, A. Morgan, N. Umpleby, V. Shah, I. Vinje, L. Štekl, C. Guasch, C. Win, G. Conroy, and A. Bertrand, 2013, Anisotropic 3d full-waveform inversion: *Geophysics*, **78**, no. 2, R59–R80, <http://dx.doi.org/10.1190/geo2012-0338.1>.